Alexandria Journal of Science and Technology

Article

Synthesis, characterization and evaluation of optically active polar semi-organic glycine-cobalt chloride crystals

Howida A. Fetouh [1,*], Ollaa M. Mailoud [2], Adly H. Elsayed [3], AH. Abu ELazm [3], Salam N. Hattawi [4], Noha Khamis [1,5], Mai S. Alsubaie [1], Riyadh H. Alshammari [6], Mohammed L. Alazmi [7]

[1] *Department of Chemistry, Faculty of Science, Alexandria University, P.O. Box 426, Alexandria 21321, Egypt.*

[2] *Department of Physics, Faculty of Science, Benghazi University, Benghazi 21861, Libya.*

[3] *Department of Physics, Faculty of Science, Alexandria University, Alexandria 21321, Egypt.*

[4] *Northern Technical University, College of Health and Medical Techniquies, Department of Renal Diaylsis Techniquies, Kirkuk, Iraq.*

[5] *Department of Chemistry, University of Warwick, Coventry, CV4 7AL, UK.*

[6] *Department of Chemistry, Faculty of Science, King Saud University, Riyadh 11421- P. O. Box 800, Saudi Arabia.*

[7] *General Science Program- Deanship of Support Studies-Alasala University-Saudi Arabia.*

[*] *Correspondence Address:*

Howida A. Fetouh: Department of Chemistry, Faculty of Science, Alexandria University, P.O. Box 426, Alexandria 21321, Egypt. Email address: howida_fetouh@alexu.edu.eg.

KEYWORDS: Slow evaporation, polar, band gap, dielectric properties.

Received:
August 02, 2024
Accepted:
August 28, 2024
Published:
October 02, 2024

ABSTRACT: Semi organic crystals of glycine Cobalt Chloride (GCC) exhibiting diverse colors were grown using the slow solvent evaporation method. The molecular structure was validated by characterization using various techniques, including Fourier-transform Infrared spectroscopy (FTIR), Mass spectra (MS), Atomic absorption spectroscopy (AAS), and powder X-ray diffraction (pXRD). Depending on the molar concentration of $CoCl_2$, the crystals exhibited a monoclinic structure with space group P21/c at low concentration and a tetragonal structure with space group P43212 at high concentration. UV-Vis. spectral analysis revealed a decrease in the lower cut-off wavelength and an increase in the band gap from 5.779 eV to 5.929 eV with the augmentation of $CoCl_2$concentration. Thermal analysis (gravimetric and differential scanning calorimetery indicated that the crystals maintain stability up to 250°C. Furthermore, the dielectric properties exhibited temperature and frequency nonlinear dependence confirming ferroelectric, piezoelectric characteristics and polarity. The good crystals' showed nonlinear optical activity and transparency in the Vis. light confirmed the possible application in the second harmonic generation.

1. INTRODCTION

Ferroelectric properties exhibited by semi organic crystals play a crucial role in various technological applications, garnering significant attention in scientific and industrial realms. Recent efforts have focused on enhancing the physicochemical properties of ferroelectric crystals, particularly those derived from the glycine amino acid. Numerous studies have been conducted involving the growth of glycine single crystals in the presence of various inorganic chloride salts such as $CuCl_2$ [1], $CdCl_2$ [2], $BaCl_2$ [3], $MgCl_2$ [4], $CoCl_2$ [5] (only one concentration), $CaCl_2$ [6], $ZnCl_2$ [7-9] and $MnCl_2$ [10-11] to enhance and modifying the crystal properties. The chemical reaction of glycine with inorganic metal chlorides was essential for expanding the crystal applications.

These ferroelectric crystals were applied in piezoelectric applications. The favorable response to large strain with low dielectric losses making these crystals suitable for applications like pyro electric detectors, memory devices and data storage [12]. Additionally, these crystals were used as thermoelectric materials, converting waste heat (from combustion sources such as pipes, automobile batteries, furnaces, and chimneys) into green electricity [13]. Hence single crystals, acting as efficient electric power generators contributing to environmental protection. With reasonably low dielectric constants and thermal stability, these

Online ISSN: 2974-3273

DOI: 10.21608/ajst.2024.309326.1044

crystals were applied in memory cells, electro-optical modulators, light deflectors, high-performance gate insulators and displays [11]. Crystals of glycine-inorganic metal chlorides showed promise for optical second harmonic generation (SHG) [14].

Glycine is a potential material for nonlinear optical (NLO) applications, possesses asymmetric chiral carbon atom (C*) facilitating interaction with light [15-16]. Semi-organic single crystals of glycine and alkali metal chlorides, exhibit optical activity and remarkable properties, including giant dielectric responses reminiscent of perovskite-type ferroelectric materials. Apart from their advantageous optical properties, these are cost-effective and capable of high-power generation [17]. The NLO properties prove useful in laser applications, where incident radiation frequencies duplicated [18]. In growth single crystals of 2 mol. % glycine-1-3 mol. % bis-thiourea-$CdCl_2$ using a slow evaporation method, the mol. percent influenced the properties [19]. The effect of $CoCl_2$ concentration on growth of glycine single crystals was not reported yet. The primary objective of this study was to investigate the impact of complexation of glycine with different concentrations of cobalt chloride [$CoCl_2$] on the (physicochemical optical, dielectric, thermal, and magnetic properties of glycine single crystals to assess their potential applications.

2. Experimental

2.1. Material and methods

All chemicals employed in this study are of analytical grade and possessed high purity. They were used in their as received state without undergoing additional purification. Glycine ($C_2H_5NO_2$) was obtained from Oxford Co. has a purity of 98.5%, while cobalt chloride hexahydrate [$CoCl_2.6H_2O$] obtained from Sigma Aldrich Co. has a purity of 97%.

The growth of glycine crystals in the presence of $CoCl_2$ was achieved following hydrothermal method [10]. Glycine and $CoCl_2$ salt with the stoichiometric molar ratio: $(C_2H_5NO_2)_{1-x}(CoCl_2)_x$ $_{(0.005,\ 0.01,\ 0.05,\ 0.08)}$ dissolved in 50 mL double-distilled water and stirred for 2.0 h at 50 rpm. The obtained supersaturated homogeneous saturated solution was filtered to remove unreacted substance. The filtrate was covered with porous aluminum foil in a dust-free environment to allow slow solvent evaporation and recrystallization at the ambient conditions of temperature and pressure [10]. The pink-colored glycine cobalt chloride poly crystals were harvested after one month and were denoted from GCC1, 2, 3, 4 in ascending order of increasing $CoCl_2$ concentration, as depicted in (**Figure 1**).

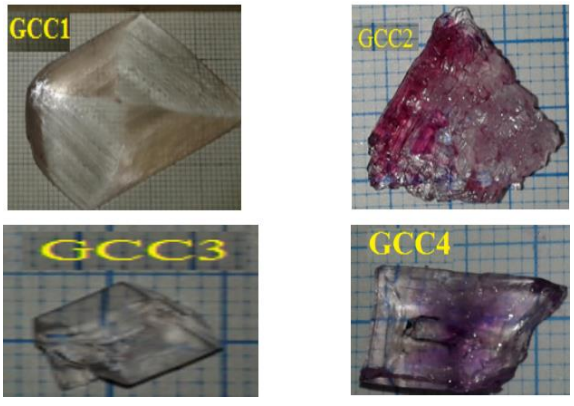

Figure 1. Observable images of glycine $CoCl_2$ poly crystals.

The GCC1 solitary crystal exhibits superior quality with the largest size, impeccable geometry and well-defined edges. The crystals GCC2 and GCC4 display a more pronounced pink color, indicating potential applications as novel colored dielectric polar materials. The polarity was attributed to the incorporated Co(II) ion, which form coordinated bonds with heteroatoms (N, O) atoms of from amino (NH_2) and carboxylate (COOH) functional groups of glycine [10].

The crystal habits changed at high [$CoCl_2$] indicated chemical reaction between glycine and $CoCl_2$ involved coordinate bond formation between hetero N, O atoms (have lone pairs electrons) of glycine (acts as Lewis base) and $CoCl_2$ acts as electrons acceptor Lewis acid (transition metal contain vacant d^7. $CoCl_2$ created defects in glycine crystals. These polycrystals lacked the equal diameter growth because low diffusion coefficient of the precursor glycine and $CoCl_2$ causes nucleation rate is more rapid than growth rate. The chemical reactions of glycine and $CoCl_2$ gave poly crystals because the requirement for growth single crystal (should maintain translational symmetry over macroscopic distances at dimensions 0.1 mm-10 cm) was invalid. The crystal quality was improved during recrystallization by allowing slow solvent evaporation and keeping the reaction vessel stagnant (undisturbed) and sealed to avoid dust or air contaminants. The crystals grown slowly from the saturated solution. The morphology changes at high [$CoCl_2$] due to ion-ion and ion-solvent interaction [19-21].

2.2. Characterization of glycine cobalt chloride crystals

The characterization techniques included [21-23]: Elemental analysis (EA) and mass spectra (MS) at the National Research Centre (NRC), Egypt. The concentration of Co(II) ion by atomic absorption spectroscopy (AAS) using Shimadzu ICH Q3D spectrophotometer. The crystallinity by powder X-ray diffractometer (Bruker AXS) with $Cu_{K\alpha 1}$ radiation (λ1.5406 Å) at 300°K; scanning range covered diffraction angles theta from 4° to 70°, a scanning step 0.02° and scanning rate 1°min^{-1}. Vibrational FTIR spectra (KBr disk) within the wavenumber range of 4000-350 cm^{-1} using a Perkin Elmer FTIR instrument (Spectrum RXI). Optical analysis using UV-Vis. spectrophotometer (Helios, Unicam) in the wavelength (λ) range of 200 nm to 1000 nm. The percentage of Co(II) uptake during recrystallization was monitored using UV-Vis. spectroscopy at λ (475 nm) and applying Beers Lambert law and was calculated using equation 1 [20]:

$$\% \text{ uptake} = (Co\text{-}Ct)/Co \times 100 \quad (1)$$

Where C_o and C_t is the concentration of Co(II) ion in the solution (mgL^{-1}) at zero and certain time respectively.

Thermal analysis through thermal gravimetric analysis (TGA) and the differential scanning calorimetry (DSC) using SHIMADZU/DSC 60 instrument under de-aerated conditions and heating rate 20°C min^{-1}. The dielectric measurements using an LCR bridge tesla 6472 over a temperature and frequency ranges of 25°C to 530°C and 100 Hz to 100 kHz respectively. The sample was compacted into a solid pellet (thickness 0.19 × 10^{-2} m and surface area 7.854 × 10^{-5} m^2), coated with highly electrically conductive silver paste for electrical contact and annealed at 120°C. Topology of GCC1 crystals was examined by surface analysis using scanning electron microscope (JSM-IT200 SEM [22]. Electron Paramagnetic Resonance (EPR)

spectra at room temperature using Jeol ESR spectrometer equipped with a sensitive standard cylindrical resonator (ER 4119 HS) and operated at a modulation frequency 100 kHz (X-band 9.43 GHz).

3. Results and discussion:

During recrystallization, [$CoCl_2$] consumed due to the coordination to glycine ligand. The chemical reaction was confirmed by linear fitting the change of [$CoCl_2$] during recrystallization to different kinetic model [20]. The linear fitting of [$CoCl_2$] to 2^o order kinetic model confirmed the chemical reaction (rate constant $6.019*10^{-8}$ $L.mol^{-1}.sec^{-1}$), (**Figure 2**).

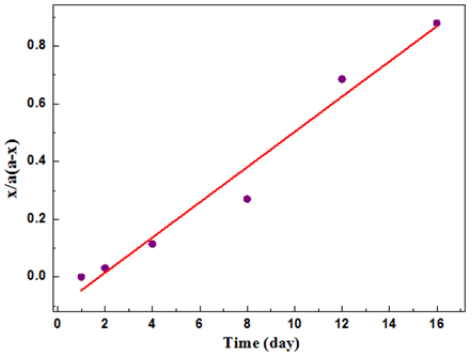

Figure 2. Linear fitting for reacted [$CoCl_2$] during recrystallization for 2^o order kinetic model.

The elemental analysis (EA) of GCC1 crystal, expressed as elemental weight percentage was provided in (Table SI.1). Converting the weight percentages into the number of moles gave the empirical ratio for elements (C, N, H, and O) as 9, 3, 12 and 13, respectively. The higher wt. % of these elements confirmed that glycine ($C_2H_5NO_2$) is the crystal matrix. The empirical molecular formula is $C_9H_{12}N_3O_{13}$. The mass MS spectra illustrated in (**Figure SI.1**) provided the end ion peaks at m/z 75.07 and 213.13 were attributed to the molecular ions of glycine and Mw. of single—crystal respectively. The incorporated [Co(II)] determined in were collected in (Table 1).

Table 1: Concentrations and absorbance of Co(II) ion in GCC crystals.

mg mL^{-1}	GCC1	GCC2	GCC3	GCC4
Concentration of Co(II) ion	0.0041	0.05326	0.046904	0.12349
[$CoCl_2$]	0.001	0.018	0.016	0.04

The lower [$CoCl_2$] than initial [$CoCl_2$] confirmed the chemical reaction gave glycine $CoCl_2$ chelate. At higher [$CoCl_2$]: 0.05-0.08 M in GCC2-GCC4, the ion-solvent interaction retarded reaction between glycine and $CoCl_2$. The high [$CoCl_2$] was ascribed to their relatively intense pink color in an irregular pattern. Comparison between observed and calculated Mw. (205.4 $gmol^{-1}$ and 213.13 respectively. The crystals structure can suggested: Co(II) central metal ion surround by glycine (N, O atoms) ligand, three water molecules, and one chloride ion through coordinate bonds formation. The solubility of the crystal in double distilled water confirmed polarity and coordinated water molecules *via* chemical reaction [23].

$CoCl_2$ acted as chemical reagent accumulated at grains of glycine crystals not a dopant replacing glycine of enter glycine crystals interstitially, as it was confirmed using SEM micrographs of the crystal GCC1 in comparison to glycine, (**Figure 3**).

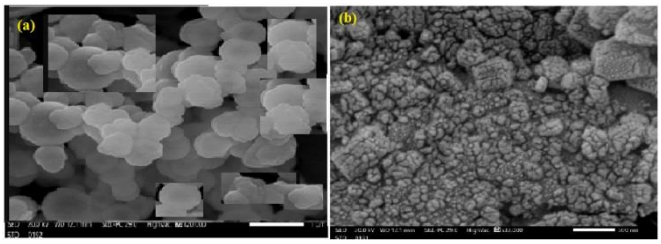

Figure 3. SEM imaging micrograph of: (a) glycine and (b) GCC1 crystal.

The homogeneous distribution of Co(II) ion over glycine crystal matrix confirmed crystal grown *via* chemical complexation reaction.

The role of $CoCl_2$ in smoothing morphology of single crystals of glycine can be explored as $CoCl_2$ acts as a habit modifier and like a buffer component (impurity) during growth of glycine single crystals. CoCl2 acts by adsorption of the chloride ion on the surface of glycine single crystal. The super saturation of glycine solution changed in the presence of CoCl2 that may changes the ionic strength of the solution without forming complexes with the glycine (crystals) or increase the ionic strength and simultaneously forms soluble complexes with glycine crystals by trapping the Co(II) ion or chloride ion. The decrease of activity of the free ions decreased the super saturation of glycine solution [23].

(Figure SI.2) depicted the powder X-ray diffraction (pXRD) patterns of GCC crystals. The sharp, strong and a dominant peak appeared at 30° in all samples confirmed good crystal quality [21].[1] Crystal GCC1 showed the highest crystallinity. The most intense peaks were shifted to lower 2-theta indicated good pillard crystallinity. Small peaks are nearly absent in GCC1, while polycrystalline regions were observed in GCC2-GCC4. (Table 2) displayed the crystalline structure type and lattice parameters. Crystal structure (contingent upon [$CoCl_2$]) and geometry aligned well with structurally related crystals reported elsewhere [3].

CIF file standard format (crystallographic information file) for exchange crystal structure data for GCC crystals were downloaded from XRD database (The International Centre for Diffraction Data (ICDD) (contain the atomic positions and the symmetry group that the crystal belongs. Rietveld refinement patterns using Full prof Suit 2018 software program, V2021 using pseudo-Voigt profile analysis. Background and peak shape were modelled with the linear fitting squares cycles and 6^{th} background polynome grade parameters at wavelength of Cu-detector and neglecting the noise and the instrumental contribution. The large number of peaks required many iterations cycles and too long iteration time consumed in

refinement GCC1 confirmed its high crystallinity and long Cartesian coordinates of unit cell and different angles in tetragonal unit cell [21]. The most intense peaks are shifted to lower 2-theta indicating increasing extent pillard crystal structure. Small peaks are nearly absent in the best crystal GCC1 and polycrystalline regions were observed in GCC2 to GCC4.

The lattice parameters correspond to the related entries in ICDD database. The calculated Miller indices (hk*l*) for each crystal confirmed the presence of regular crystalline planes at different intersections with Cartesian coordinates x, y, z. Both crystals GCC1 and GCC2, [$CoCl_2$] 0.005M, 0.05M exhibited a monoclinic crystalline system and belonged to space groups P21/c and P21 respectively. The difference in space group was due to [$CoCl_2$] affect symmetry elements of the crystals [21].

The crystals GCC3 and GCC4 (0.05, 0.08M $CoCl_2$) respectively displayed a tetragonal structure of the same space group (P43212). The shift in structure from monoclinic to tetragonal symmetry was attributed to the phase transformation from α glycine to γ glycine with increasing [$CoCl_2$]. All reflection peaks corresponding to different crystal planes were indexed. The relative peak intensity was recorded in (Table SI.2). Theoretical simulations of pXRD patterns corresponding to PDF cards were performed using FullProf software program V2021 providing diffraction angles ($2\theta_{Calc.}$) and spacing distances ($d_{Calc.}$) between each pair of adjacent crystalline plane. Increasing [$CoCl_2$] from (0.005, 0.01M) to 0.05M, 0.08M caused phase transition from the monoclinic structure (α glycine) in GCC1 and GCC2 to the tetragonal γ-glycine in GCC3 and GCC4 at $CoCl_2$ and slight change in the position of glycine diffraction peak from (2θ = 23.9° to 25°) [10].

Table 2 :Lattice parameters for GCC single crystals.

Sample name, [$CoCl_2$]		GCC1 (0.005)	GCC2 (0.01)	GCC3(0.05)	GCC4(0.08)
Reference PDF card		00-016-0472	00-023-1605	00-030-1628	00-023-1604
Crystal system		Monoclinic		Tetragonal	
Space group of symmetry and glycine phase		P21/C	P21	P43212	
		Alpha		Gamma	
Unit cell parameters	Dimensions (Å)	a 10.68, b 7.890, c 9.090	a 8.00, b 8.772, c 7.032	a= b = 9.682 c 16.287	a= b=17.953 c 24.213
	Angles (°)	α = γ = 90 β =110.40	α = γ = 90 β =107.03	α= β = γ =90	
	Volume ($Å^3$)	717.931	417.839	1526.762	7817.137
Density (calc.) g, cm^{-3}		1.656	1.23	1.521	1.35

The density of the crystals followed the order: GCC1 > GCC3 > GCC2 > GCC4. This trend confirms the condensed crystalline state in the same order and corroborates the pink color of crystals. High [$CoCl_2$] increases the volume of the unit cell. In comparison to a related reported study on bis-glycine cobalt chloride, monoclinic system with a centrosymmetric space group [21].

The FTIR spectra of GCC1-GCC4 single crystals were presented in (**Figure SI. 3(a-d)**). All vibrational frequencies of functional groups were assigned. For GCC1, the strong vibrational band due to the bending and rocking of COO^- group (607 cm^{-1}, 502 cm^{-1}). The strong peak at 893 cm^{-1} (CNN symmetric stretching). The asymmetric stretching of anharmonic oscillator C-N bond (1032 cm^{-1}). For COO^- group: symmetric stretching and asymmetric stretching at 1330 cm^{-1} and 1511 cm^{-1} respectively. A low-intensity peak at 2124 cm^{-1} (asymmetric stretching of N-H in NH_3^+. The absorption band at 2614 cm^{-1} (O-H stretching of the hydrogen-bonded carboxyl group deformation [5]. The NH_3^+, NH_2 stretching vibrational band appeared at 2892cm^{-1} and 3921 cm^{-1} respectively. The free stretching of the NH_2 group at 3653 cm^{-1}. The IR spectra of GCC2, GCC3, and GCC4 samples showed the same functional groups as GCC1, with a small shift in the wavenumber (Table SI. 3).

The optical percentage transmittance GCC crystals were depicted in (**Figure 4**). The crystals exhibited high optical transparency in UV-Vis. Region. The corresponding Tauc's plots presented were constructed and the band gaps (Eg) were determined by extrapolation the linear portion to the x-axis at zero value of $(\alpha h\nu)^2$ using micro calculation origin software program.

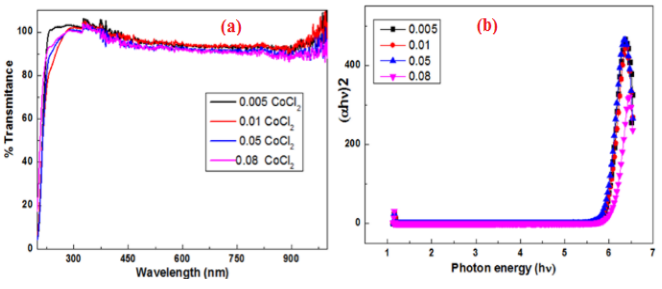

Figure 4. Variation of: (a) Transmission and (b) Tauc's plots of GCC crystals with photon energy.

All samples showed up to 100% transmittance in UV-Vis. region of electromagnetic radiation with the crystal (0.005M $CoCl_2$) is the best transparent sample. The values of Eg and cutoff wavelengths were collected in (Table SI.4). The large band gap indicated that the crystals completely transmitted UV and Vis. light and exhibited good non-linear optical activity at the wavelength range 400-1200 nm [23]. The values Eg for GCC1, GCC2, GCC3, and GCC4 crystals were found to be 5.779, 5.806, 5.767, and 5.929 eV, respectively in comparison to glycine (3.16 eV). These new grown crystals exhibited a high Eg a property that is particularly advantageous for applications in the field of UV-tunable lasers [11]. The values of Eg of GCC crystals increased with increasing [$CoCl_2$], suggesting that Co(II) ion enhanced the transparency of glycine crystals.

The optical parameters, including absorption coefficient (α), reflectance (R), refractive indices (n), extinction coefficient (k) and the electric susceptibility (χ), were computed using equations (1-6): [24-26].

$$k = \frac{\lambda\alpha}{4\pi} \quad (1)$$

$$R = \frac{1 \pm \sqrt{1-\exp(-\alpha t)+\exp(\alpha t)}}{1+\exp(-\alpha t)} \quad (2)$$

$$n = -\left(\frac{(R+1) \pm \sqrt{-3R^2+10R-3}}{2(R-1)}\right. \quad (3)$$

$$K = \frac{\lambda\alpha}{4\pi} \quad (4)$$

$$\chi = \frac{n^2-K^2-\epsilon_0}{4\pi}$$

Where λ: wavelength, α is the optical absorption coefficient, t: sample thickness,

ε_o : Permittivity of free space (8.85 x 10^{-12} Fm^{-1}). (6)

Plots of extinction coefficient and reflectance against photon energy were shown in (**Figure 5**). The observed nonlinear variation suggests the potential use of this material in the fabrication of optical and thermal devices and lasing applications [15].

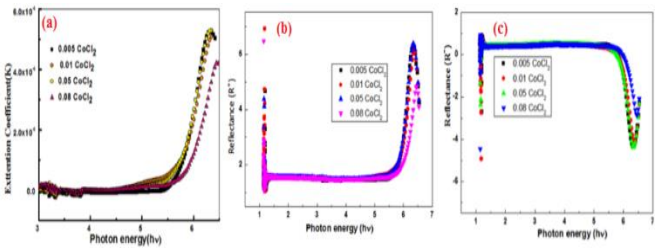

Figure 5. Variation: (a) extinction coefficient, (b) and (c) reflectance of GCC crystals with photon energy.

The values of (k) increased with increasing photon energy and are low indicated that less light lost by scattering and the absorption per unit distance passing through GCC crystal. The low values reflectance (R) showed little reflection of incident solar radiation back into space and the most of electromagnetic radiations transmitted through the sample crystals [10, 21, 23].

The plots of refractive index (n) and electrical susceptibility (χ) against photon energy were presented in (**Figure 6**).

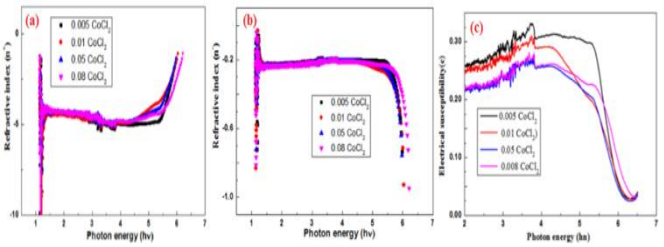

Figure 6. Variation refractive index and electrical susceptibility of GCC crystals versus photon energy.

The negative value of refractive index (n) depends on the angles of incidence or refraction of light indicating the GCC crystal are meta-materials (allow light bent "backward" at a negative angle of refraction, used in control and molding the flow of light waves, would function as analog computers operating with light energy rather than electricity (advantageous in science and engineering, more faster than their digital counterparts, while operate at less power consumption [10].

The positive value of electrical susceptibility (χ) that is a dimensionless proportionality constant indicating *polarization of the dielectric crystal in an applied electric* field. All GCC crystal exhibited favorable χ values indicating a high potential for laser emission. The best polarization was shown by crystal GCC1 (0.005M $CoCl_2$) followed by sample GCC2. The high [$CoCl_2$] decreased χ because of decreasing crystal symmetry in agreement with pXRD diffraction parameters (from tetragonal to monoclinic space group of symmetry

Increasing [$CoCl_2$] influenced the optical properties of GCC crystals. The positive values of χ, optical activity to UV light, and transparency to Vis. light, indicating suitability for second harmonic generation (SHG) where fundamental laser beam of incident laser light photons (hυ) (frequency (υ) doubling) on interaction with the crystal emits new photons with (2υ or 0.5λ) of the incident photon (SHG). The large χ of polar GCC confirmed careful aligned interfaces, creating dipoles for phase matching and causing frequency multiplication, as illustrated in outline below.

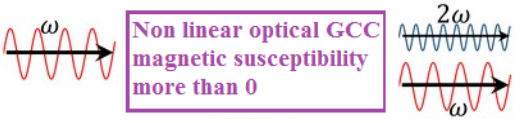

Schematic representation of frequency duplication in GCC ~~single~~ crystals

On irradiation with nanosecond ultra-fast laser photon of energy (hυ), free electrons are converted into phonons transfer heat. Upon vibrational relaxation of phonons from higher infinite vibrational levels (containing infinite rotational energy levels in between). Based on this photo physical processes, phonons are emitted as coherent laser beams with multiplied frequency (υ) creating SHG (coherent laser beam light emitted). In second-harmonic generation process, an input wave of fundamental frequency (υ), in passing through a nonlinear polar crystal produces an output wave of second harmonic frequency (2υ).

The nonlinear χ tensor reflects molecular orientation at crystal

edges caused frequency multiplication. On irradiation, all electrons underwent vibrational oscillation to higher energy levels causing thermal heating of the crystals. SHG in GCC crystals was evident from pXRD patterns and crystal parameters, which demonstrate an ordered geometry of non-centrosymmetric structures in monoclinic or tetragonal unit cells. This confirmed that, on irradiation crystal with a specific wavelength (λ) and incident angle (θ), the order (n) of any crystalline planes (inter planner distance (d)) matched according to the Bragg condition [23]:

$$n\lambda = 2\ d^* \sin \qquad (7)$$

The incident light undergoes coherent interference between wave functions of delocalized free electrons in crystals.

Differential scanning calorimetric analysis (DSC) of GCC sample were shown in (**Figure. 7**). The sharp endothermic peak at confirming good crystallinity and corresponding to the decomposition of glycine [23].The GCC1 sample is the purest crystal because it displayed a very sharp and narrow DSC peak along with a relatively high decomposition point at 253.34ºC. No phase transformation was observed for each crystal confirmed pXRD diffraction patterns that showed each crystal exhibited only one crystalline morphology [21].

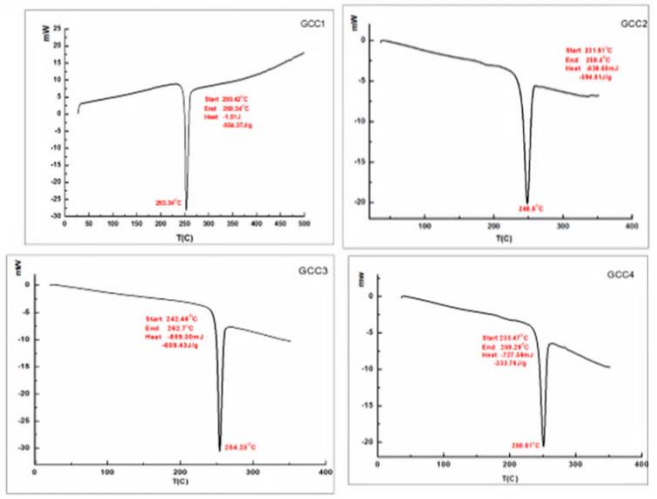

Figure 7. Thermal response (TGA and DSC) of GCC crystals.

DSC analysis indicated that GCC crystals exhibit a distinct melting point (Table SI. 5), suggesting high purity and thermal stability. GCC1, in particular, demonstrated the highest decomposition temperature, reaching 500°C [21, 26].

The plan dielectric measurement for the best GCC1 crystal was to evaluate crystal polarity. (**Figure 8**) depicted the dielectric permittivity constant (ε) at temperature range of 350-520ºK (up to decomposition temperature. The total ε and its real (ε′) and the imaginary (ε″) components as well as dielectric loss ($\tan\delta$) and AC conductivity (σ_{AC}) were calculated using equations 7-10 respectively [27-29].

$$\varepsilon = \frac{Cd}{\varepsilon_o A} \qquad (8)$$

$$\varepsilon' = |\varepsilon| \cos\theta \qquad \varepsilon'' = |\varepsilon| \sin\theta \qquad (9)$$

$$\text{Dielectric loss } or\ loss\ tangent\ (\tan\delta) = \frac{\varepsilon''}{\varepsilon'} \qquad (10)$$

$$\sigma AC = 4\pi \times \varepsilon'' \times \varepsilon' \times \omega \qquad (11)$$

Where C, d, A are sample (capacitance, thickness and cross sectional area); ω : angular frequency $(2\pi f)$ and f is the linear frequency (Hz).

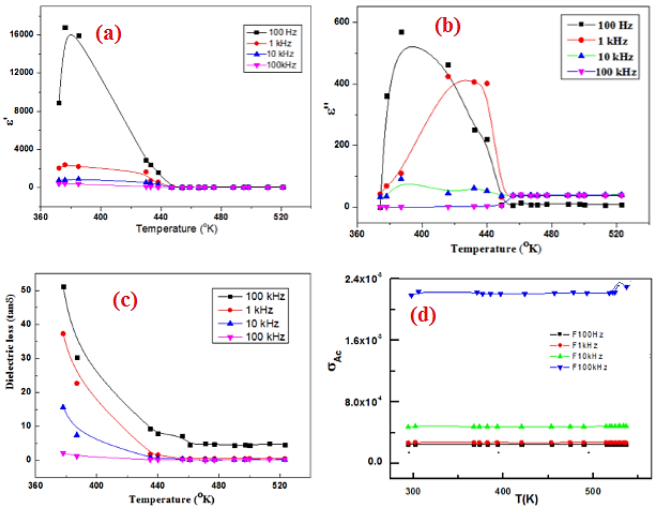

Figure 8. Variation: (a)ε′ , (b) ε″, (*c*) ($\tan\delta$), (d) σ_{AC} of GCC1 crystal with frequency and temperature.

At low 100 kHz, high ε values (depend on the atomic arrangement) due to polarization (ionic and electronic) and space charge orientation [30]. Polarization enhanced optical activity, reduced crystal lattice defects and confirmed the polarity enabled application as charge storage reservoirs electrical double layer (EDL) capacitor created by the organized and regularly repeating atomic structure held together by chemical bonds in the unit cells [31].

The nonlinear variation in dielectric properties with increasing temperature and frequency (applied strains) confirmed ferroelectricity. Decrease ε with rising temperature confirmed piezoelectricity. ε′′ sharply increase with temperature at low frequency then limited at high frequency [30]. The change in dielectric loss ($\tan\delta$) (depends on both ε′and ε″) has high values at 100Hz and low values at 100 kHz confirmed the piezoelectricity (energy conservation by conversion mechanical energy into electricity or vice versa without energy dissipation and sustained energy storage). The gradual decrease was caused by the lattice defects [10, 31].

The loss tangent($\tan\delta$) results from absorption of electromagnetic radiation (waves have particle like characters) by the dielectric glycine crystals. material and depends on the material's structure and glass-resin composition. The low value of loss tangent results confirmed targeting the arrival of more of the original transmitted signal [10, 31].

Significant AC conductivity (σ_{AC}) confirmed polarization [32.33] due to the mobility of charge carriers, specifically delocalized free electrons in the crystal lattice increased at low frequency. The σ_{AC} diminished at high frequencies, signifying crystal polarization in applied AC potential (ferroelectricity). The ionic mobility enhanced with heating, albeit the slight increase in σ_{AC}

was due to reduction in the thickness of EDL. The majority of electrons thermally vibrate as simple anharmonic oscillators and converted into phonons. The nonlinear variation in ε and σ_{AC} with the applied frequency confirmed polarity that enabled applications as charge storage capacitors and construction of radio frequency transmission lines [21, 23].

Electron paramagnetic resonance (EPR) of GCC1 spectra was depicted in (**Figure SI.4**). A distorted anisotropic signal, accompanied by an anisotropic weak shoulder on the high field side, indicates the presence of some Co(II) ions in the crystal lattice [32-34]. Various calculated parameters, such as ΔH(G), Ho(G), and g-values were listed in (Table SI.6). Also the higher g-factor for than that of free electrons indicated the presence of Co(II) ions [35]. The line width (ΔH 885.6 G) suggests a strong exchange magnetic interaction between Co(II) ions. The weak hyperfine structure was attributed to the low [$CoCl_2$] used in this crystal. Therefore, recording the ESR signals of GCC requires appropriate operational conditions of temperature and microwave power to ensure a good signal-to-noise ratio, compensating background signals and considering integer spin signals. These findings was aligned with those observed for Co(II) crystals in EPR studies[35], where EPR signals exhibited a broad envelope when using frequency modulation restricted to ~10 GHz (much lower than the line width of the signal). Consequently, high [Co(II)] ions are necessary for achieving accuracy in recording ESR spectra [10].

Glycine single crystals widely applied in all fields of technology [1-4]. Gelatin is a sustainable biodegradable biopolymer (from animal sources) and safely used in foods, medication and cosmetics. Gelatin obtained by the partial hydrolysis of the collagen triple helix n protein abundant in skin, bones, connective tissues and hides. Chemical structure of gelatin can be represented as shown in (**Figure 9**).

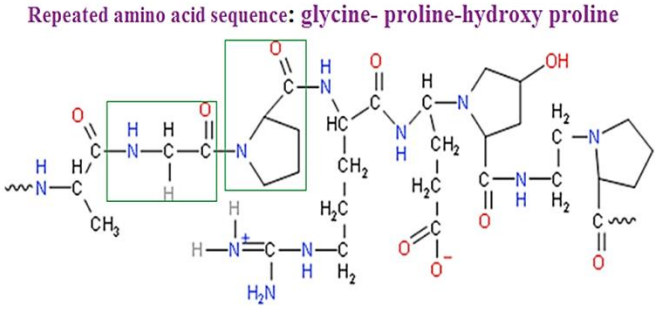

Figure 8. Sustainable gelatin polymer (glycine source).

Gelatin dissolve in water by warming at 40°C. Glycine amino acid can be obtained from gelatin using high performance liquid chromatography (HPLC) [36]. Glycine separation of glycine from proline and hydroxyl proline using number of solvents and *via* passing the mobile phase containing gelatin through a finely divided stationary phase under high pressure. For separation of glycine by ion exchange chromatography, in more basic medium than the isoelectric point ($pH_{zero\ charge}$). The protonated amino (NH_3^+) group of glycine loses proton to form anion and can be separated using anion exchange resin. The activity of the used adsorbents in column chromatography follows the order:

Charcoal > magnesium carbonate > silica gel

Gas liquid chromatography (GLC) is a suitable technique used for qualitative identification and quantitative measurements respectively. The quantitative is based on the retention time and peak area. The retention or capacity factor is a parameter used to compare the relative migration rates of amino acids along the column [37].

In comparison with previous studies of biologically active and antitumor proline single crystals, $CoCl_2$ affect single crystals of proline [23] and glycine [this study] gave different colored crystals. The polarity of these crystals was confirmed by AC electrical conductivity [23] and solubility in water.

The semi organic nature of amino acids (glycine and proline) single crystals suggested good thermal and electrical conductivities. These solid electrolytes could be used in energy storage and saving devices. Polar thermo-electric crystals change electrical and thermal properties on heating without decomposition before T_C. The partially filled d-orbitals of Co(II) ion is the controlling factors. The Ferro electricity is due reoriented spontaneous polarization (P_s) by atomic displacements, its direction conforms to crystal symmetry, its restrictions similar to pyroelectric crystals. Maximum P_s below T_C declined at T_C. However, if high-temperature phase is polar, P_s minimalized at T_C; if another phase forms at lower temperature, P_s increase or diminish below phase transition. In 1° ferroelectric-paraelectric phase transition, P_s maximized at T_C. In 2° order phase transition, P_s decreases gradually on approaching T_C [38].

4. Conclusion

High-quality, transparent single crystals of glycine cobalt chloride were successfully grown using the slow evaporation method at room temperature. The crystals exhibited different colors based on the percentage of $CoCl_2$. Monoclinic and tetragonal crystal structures were obtained at lower and higher concentrations, respectively. UV-Vis spectra revealed λ-cutoff values for GCC1, GCC2, GCC3, and GCC4 single crystals at 216 nm, 222 nm, 224 nm, and 214 nm, respectively. These crystals demonstrated broad transparency in the near-infrared region of the electromagnetic spectrum. The high dielectric constants at low frequencies indicating their potential in optical, perovskite, and ferroelectric applications. The crystals exhibited thermal stability up to 230°C. AC conductivity and low dielectric loss suggested excellent optical and electrical properties. The EPR spectra indicated isotropic paramagnetic properties. The crystals featured various functional groups. These crystals were transparent in the λ range of 265 nm to 1100 nm. The dielectric properties, loss tangent and AC conductivity varied with frequency and the crystals exhibited thermal stability up to 220°C.

Supporting Information Summary:

Comprising all remaining data and materials from this investigation.

Ethics approval and consent to participate

No ethical issue in manuscript. Authors approved consent on participation.

Consent for publication

Authors approved consent on publication.

Availability of data and materials:

"All data generated or analyzed during this study are included in this published article".

Declaration of interests

Authors declared no conflict of interest have influenced the submitted work. There is no known competing financial interests or personal relationships that could have appeared to influence the work reported in this research article**.**

References

[1] Sudha, S.; Sathya, T.; Raj, M. J. Studies on thermal, microhardness and di-electric properties of glycine nickel chloride. Int. J. Sci. Technol. Res. 2012, 1, 35-37.

[2] Selvakumar, P. N.; Subbulakshmi, V. P. Subramanian, P. An EPR and optical study of VO2+ in bis (glycine) cadmium chloride single crystals. Zeitschrift für Naturforschung A. 2007, 62, 462-466.

[3] Pandian, M. S.; Ramasamy, P. Growth and characterization of solution-grown tetra glycine barium chloride (TGBC) single crystals. J. Cryst. Growth. 2008, 310, 2563-2568.

[4] Dillip, G.; Bhagavannarayana, G.; Raghavaiah, P.; Raju, B. D. P. Effect of magnesium chloride on growth, crystalline perfection, structural, optical, thermal and NLO behavior of γ-glycine crystals. Mater. Chem. Phys. 2012, 134, 371-376.

[5] John, J.; Christuraj, P.; Anitha, K.; Balasubramanian, T. Band gap enhancement on metal chelation: Growth and characterization of cobalt chelated glycine single crystals for optoelectronic applications. Mater. Chem. Phys. 2009, 118, 284-287.

[6] Thiyagaraj, S.; Meenakshi, G. Synthesis, growth of semiorganic TGDCC (Tetra Glycine Dihydrated Calcium Chloride) single crystal and a study of effect by Urea on the structural and optical properties. J. Appl. Phys. 2013, 2, 25-30.

[7] Sugandhi, K.; Verma, S.; Jose, M.; Joseph, V.; Das, S. J. Effect of pH on the growth, crystalline perfection, nonlinear optical and mechanical properties of tris-glycine zinc chloride single crystals. Opt. Laser Technol. 2013, 54, 347-352.

[8] Arivuoli, S. S. D. Synthesis, optical and dielectric properties of tris-glycine zinc chloride (TGZC) single crystals. J. Met. Mater. Miner. 2011, 10, 517-526.

[9] Ramteke, S. P.; Anis, M.; Baig, M.; Pahurkar, V.; Muley, G. Optical and electrical analysis of Cu+2 ion doped zinc thiourea chloride (ZTC) crystal: An outstanding 30× 24× 04 mm3 bulk monocrystal grown from pH controlled aqueous solution. optik, 2017, 137, 31-36.

[10] Mailoud, O. M.; Elsayed, A. H.; El Fetouh, H. A.; ELazm, A. A. Synthesis and characterization of paramagnetic isotropic glycine manganese chloride single crystal with various dopant concentrations. Results Phys. 2019, 12, 925-933.

[11] Alemu, D.; Firehun, S.; Abza, T.; Peter, M. E. The Study of Structural, Optical, and Dielectric Properties of Magnesium Chloride-Doped Triglycine Sulphate Ferroelectric Single Crystals. Adv. Mater. Sci. Eng. 2022, 2421382-2421388.

[12] Troiler-McKinstry, S. Impact of ferroelectricity. Am. Ceram. Soc. Bull. 2020, 99, 22-23.

[13] Fan, Y.; Tan, G. Ferroelectric engineering advances thermoelectric materials. Mater. Lab, 2022, 1, 220008-220012.

[14] Chung, In; Mercouri G. Kanatzidis. Metal chalcogenides: a rich source of nonlinear optical materials. Chem. Mater. 2014, 26, 849-869.

[15] Bhat, M. N.; Dharmaprakash, S. New nonlinear optical material: glycine sodium nitrate. J. Cryst. Growth. 2002, 235, 511-516.

[16] Balamurugan, M.; Boobalan, S.; Subramanian, P. EPR Studies of Cu(II) ION Doped In Hexaaquazinc Tetraaquabis (Glycine) Zincsulfate Single Crystal. Int. J. Sci. Res. 2016, 8, 38-42.

[17] Yao, F.; Peng, J.; Li, R.; Li, W.; Gui, P.; Li, B.; Liu, C.; Tao, C.; Lin, Q.; Fang, G. Room-temperature liquid diffused separation induced crystallization for high-quality perovskite single crystals. Nature communications. 2020, 11, 1194-11113.

[18] Vizhi, R. E.; Yogambal, C.; Babu, D. R. Influence of sodium formate in γ-glycine single crystals–synthesis, growth and characterization. Optik. 2015, 126, 77-80.

[19] Dhumane, N.; Hussaini, S.; Dongre, V.; Karmuse, P.; Shirsat, M. Growth and characterization of glycine doped bis thiourea cadmium chloride single crystal. Crystal Research and Technology: J. Exptl. Ind. Crystallogr. 2009, 44, 269-274.

[20] Al Harby, N.F.; Fetouh, H.A.; El-Batouti, M., Facile green synthesis route for new ecofriendly photo catalyst for degradation acid red 8 dye and nitrogen recovery. Scientific Reports. 2024, 14, 1091-1109.

[21] Almufarij, R.S.A.; Ali, A.E.D.; Elba, M.E.; Okab, H.E.; Mailoud, O.M., Abdel-Hamid, H.; Fetouh Elsayed, H.A. Growth of New, Optically Active, Semi-Organic Single Crystals Glycine-Copper Sulphate Doped by Silver Nanoparticles. Applied Nano. 2023, 4, 115-137.

[22] Mailoud, O. M.; Elsayed, A. H.; Abo-Elazm, A.; Fetouh, H. Synthesis and study the structure, optical, thermal and dielectric properties of promising Glycine Copper Nitrate (GCN) single crystals. Results in Phys. 2018, 10, 512-520.

[23] Almufarij, R.S.; Ali, A.E.; Elbah, M.E.; Elmaghraby, N.S.; Khashaba, M.A.; Abdel-Hamid, H.; Fetouh, H.A. Preparation, characterization of new antimicrobial antitumor hybrid semi-organic single crystals of proline amino acid doped by silver nanoparticles. Biomedicines. 2023, 11, 360-381.

[24] Sahebi, R. Comment on: " Investigation on nucleation kinetics, growth, optical, mechanical, conductivity and Z scan studies on thiosemicarbazide cadmium chloride monohydrate (TSCCCM) single

crystals for nonlinear applications". J. Mater. Sci. Mater. Electron. 2019, 30, 15116-15129 .
[25] Ramezan S.; Pichan, K.; Kamalesh, T.; Senthilpandian, M.; Ramasamy, P. Crystal Growth and Physico-Chemical Characterization of Semi-Organic [C4H12N2] ZnCl4. H2O Single Crystal for Laser Applications. Chin. 2021, J. Phys. 66, 109-111.
[26] Hassanien, A. S.; Aly, K.; Akl, A. A. Study of optical properties of thermally evaporated ZnSe thin films annealed at different pulsed laser powers. J. Alloys Compd. 2016, 685, 733-742.
[27] Debasis, D.; Tanmay, G. K.; Panchanan, P. Studies of dielectric characteristics of BaBi2Nb2O9 ferroelectrics prepared by chemical precursor decomposition method. Solid State Sci. 2007, 9, 57-64.
[28] Packiya Raj, M.; Ravi Kumar, S.; Srineevasan, R.; Ravisankar, R. Synthesis, growth, and structural, optical, mechanical, electrical properties of a new inorganic nonlinear optical crystal: Sodium manganese tetrachloride (SMTC). J. Taibah Univ. Sci. 2017, 11, 76-84.
[29] Karolin, A.; Jayakumari, K.; Mahadevan, C. Growth and characterization of pure and Ni2+ doped glycine sodium sulfate crystals. Int. Res. J. Eng.Technol. 2013, 2, 646-651.
[30] Abd-El-Nabey, B.A.; Eldissouky, A.; Fetouh, H.A.; Mohamed, M.E. Role of anion in the electrochemical dissolution of copper and its inhibition by diethyl dithiocarbamate in neutral aqueous solutions. Phys. Chem. 2018, 8, 1-12.
[31] Vizhi, R. E.; Yogambal, C. Investigations on the growth and characterization of γ-glycine single crystal in the presence of sodium bromide. J. Cryst. Growth. 2016, 452, 198-203.
[32] Jebli, M.; Rayssi, C.; Dhahri, J.; Henda, M.B.; Belmabrouk, H.; Bajahzar, A. Structural and morphological studies, and temperature/frequency dependence of electrical conductivity of Ba0.97 La 0.02 Ti 1− x Nb 4x/5 O3 perovskite ceramics. RSC advances. 2021, 11, 23664-23678.
[33] Chennakrishnan, S.; Ravikumar, S.; Sivavishnu, D.; Raj, M. P.; Varalakshmi, S. Investigation on Pure and L-lysine Doped (Tri) Glycine Barium Chloride (TGBC) Single Crystal for Nonlinear Optical Applications. Mech. Mater. Sci. J. 2017, 8, 1-10.
[34] EL-Fadl, A.A.; Abdulwahab, A.M. The effect of cobalt-doping on some of the optical properties of glycine zinc sulfate (GZS) single crystal. Physica B: Condensed Matter. 2010, 405, 3421-3426.
[35] Ceylan, Ü.; Tapramaz, R. The EPR study of Mn2+ ion doped KBr and VO2+ ion doped KH2PO4 under high pressure. Spectrochim. Acta Part A: Molecular and Bimolecular Spectroscopy. 2016, 152, 654-657.
[36] Russell, J.D.; Dolphin, J.M.; Koppang, M.D. Selective analysis of secondary amino acids in gelatin using pulsed electrochemical detection. Analytical chemistry.2007, 79, 6615-6621.
[37] Mega, T.; Matsushima, Y. Affinity Chromatography of Glycosidases Preparation and Properties of Affinity Column Adsorbents. J. Biochemistry. 1976, 79, 185-194.
[38] El Batouti, M.; Fetouh, H.A. A facile new modified method for the preparation of a new cerium-doped lanthanium cuperate perovskite energy storage system using nanotechnology. New J. Chemistry. 2021, 45, 8506-8515.